AN INVESTIGATION ON HYBRID INTERFACE USING ON-LINE MONITORING EXPERIMENT AND FINITE ELEMENT ANALYSES

Hieu T.X. Truong[1], Marcias J. Martinez[2], Ozden O. Ochoa[3] and Dimitris C. Lagoudas[4]

[1]Mechanical Engineering Department, Texas A&M University
3123 TAMU, College Station, Texas 77843-3123, United States
Email: hieutruong@tamu.edu

[2]Faculty of Aerospace Engineering, Delft University of Technology
Building 62, Kluyverweg 1, 2629 HS Delft, P.O. Box 5058
2600 GB Delft, The Netherlands
Email: m.j.martinez@tudelft.nl

[3]Mechanical Engineering Department, Texas A&M University
3123 TAMU, College Station, Texas 77843-3123, United States
Email: oochoa@tamu.edu

[4]Aerospace Engineering Department, Texas A&M University
3141 TAMU, College Station, Texas 77843-3141, United States
Email: lagoudas@tamu.edu

Keywords: Double Cantilever Beam (DCB), High Temperature, Finite Elements, Fiber Optics, Hybrid Interface

ABSTRACT

In this work, the hybrid interface between metal and thermosetting polymer matrix composite was studied via experimental and numerical investigations. Hybrid laminates, whose constituents are aluminum foil, carbon fabric and epoxy matrix, were manufactured using the vacuum assisted resin transfer molding process. Chromic anodization was used to treat the surfaces of the aluminum foil prior to fabricating the hybrid laminates. The mode-I dominated delamination behavior was studied using the double cantilever beam tests at both room (25^{o}C) and elevated (60^{o}C) temperatures. Distributed strain profiles were measured on both the top and bottom of the specimen using Rayleigh backscattering fiber optics technique. Finite element analysis was performed to assist with the analysis and interpretation of experimental results. Load-displacement and strain profiles measured from experiments were compared with values obtained numerically. Good agreements between the experimental and numerical results were observed.

1 INTRODUCTION

Fiber metal laminates (FMLs) that are composed of alternating metal and fiber reinforced polymer matrix composite (PMC) layers were developed at Delft University of Technology and since then have found many practical applications [1]. FMLs with aluminium as the metallic reinforcement layer have been widely studied and used in composites referred as GLARE (glass fiber and aluminium reinforced composites) and CARALL (carbon fiber and aluminium reinforced composites). Most of the FMLs investigated so far were created using composite pre-pregs and cured in autoclaves. This method of manufacturing is very expensive; hence, there is a need to explore out-of-autoclave methods to fabricate FMLs in a more cost-effective way.

In FMLs, the bonding and delamination at the hybrid metal-PMC interfacial regions is of critical concern. There has been considerable research emphasis on the fatigue damage and delamination behavior in these hybrid composite systems [2, 3]. However, quasi-static fracture toughness of the hybrid interface in FMLs has not received much attention. The mode I and mode II fracture toughness of hybrid Al/CFRP interface was studied experimentally and computationally by Ning *et al* [4, 5]. The effect of nano-reinforcement (carbon nanofiber) on the improvement of fracture toughness was investigated in their work. However, they did not account for the mode mixity present at the hybrid interfaces during crack propagation nor consider the influence of elevated temperature on the fracture behavior. Banea and colleagues have studied temperature-dependent fracture toughness of adhesive joints via both experimental and numerical investigation [6, 7]. The work of Banea *et al*, however, only dealt with adhesive joints of metal-to-metal such as stainless steel substrates.

The double cantilever beam (DCB) test has been widely used to investigate the mode I fracture toughness in composite laminates. Our previous work based on traditional DCB tests of the hybrid metal-PMC interfaces at room and high temperature enabled us to capture the delamination progression via optical cameras [8]. The numerical analysis of DCB results has been performed assuming a uniform delamination front across the specimen width. However, in reality, the crack front is not always straight and the crack does not always propagate uniformly across the width as proven by the finite element analysis results [9]. Thus, in-situ non-destructive testing methods should be explored to experimentally monitor the crack front profile upon propagation.

Herein we introduce our current approach where the hybrid composite laminate was fabricated using an out-of-autoclave method. The vacuum assisted resin transfer molding (VARTM) technique was used to prepare panels for DCB specimens. The layup consisted of one single layer of aluminium foil sandwiched between eight layers of carbon fabric on the top, and eight layers of carbon fabric on the bottom in an epoxy matrix. An initial crack for the hybrid metal-PMC interface was created by placing an FEP film on one side of the metal layer. The DCB test was used to investigate the mode I fracture toughness of the hybrid metal-PMC interface at room and elevated temperatures. Furthermore, in-situ delamination monitoring using Rayleigh backscattered distributed sensing fiber optics was performed during the DCB test to capture the strain distribution and thus analyse the length and location of the crack front. Finite element analysis (FEA) was performed on the hybrid DCB specimen. Axial strain profiles along the DCB beam's length were obtained from FEA results at the top and bottom surfaces at different time steps during crack propagation. The strain and load-displacement predictions obtained from FEA were validated via comparison with strain data obtained from the fiber optic system and experimental load-displacement measurement.

2 HYBRID LAMINATE FABRICATION

2.1 Materials

The constituent materials for hybrid laminates investigated in this study are 3K plain weave T300 carbon fabric, aluminium foil 0.4 mm thick and an epoxy Epikote-Epikure 04908 matrix. The reinforcement was laid up in the following configuration: $[0]_8/\mathrm{Al}/_{\mathbf{PCF}}/[0]_8$. It should be noted that even though the composite panel's reinforcements are not unidirectional laminae but rather carbon fabric layers, the notation 0 is adopted to show that the fabric layers are oriented in direction along the warp yarns. A 12 μm thick fluorinated ethylene propylene (FEP) film was placed adjacent to one side of the Al foil to create the initial crack. This layer is denoted as pre-crack film (PCF) in the layup. The carbon fabric layers were prepared such that they are wider and longer than the Al foil an amount of 20 mm and 30 mm in the width and length dimensions respectively. This was done to avoid damage of the vacuum bag caused by sharp edges of the Al foil that can create leakage during infusion and curing. Table 1 shows a summary of dimensions and quantities of different layers used in the laminate.

2.2 Hybrid laminate processing

Surface treatment was done on Al surfaces to create good adhesion with the epoxy matrix. Chromic acid anodization was performed, followed by priming with BR-127 primers. To ensure that the resin wet the entire laminate, both on the top and bottom sides with respect to the Al foil placed at the center, the layup was performed so that two independent infusion flows were created. Although the resin flow on the topside is separated from that of the bottom side, one resin inlet and one resin outlet were used for the entire panel. One flow mesh was placed on the bottom and one was placed on the top of the panel preform. The two flow-mesh layers met at the resin inlet tube. Two peel ply layers separated the top and bottom flow mesh layers from the panel. A vacuum bag was placed on top of the bottom 8-layer carbon fabric stack and adjacent to the initial crack film to separate the top and bottom flow. The dashed blue lines on Figure 1(a) highlight the edges of this vacuum bag. Figure 1(b) shows the layup after the Al foil was assembled.

Material	Number of layers	In-plane dimensions (mm x mm)	Thickness (μm)
Plain weave T300 carbon fabric	16	220.0 x 330.0	253.1 (thickness of each cured layer)
Al foil	1	200.0 x 300.0	400.0
FEP film	1	110.0 x 360.0	12.5

Table 1: Dimensions and number of layers of materials used in the hybrid laminate.

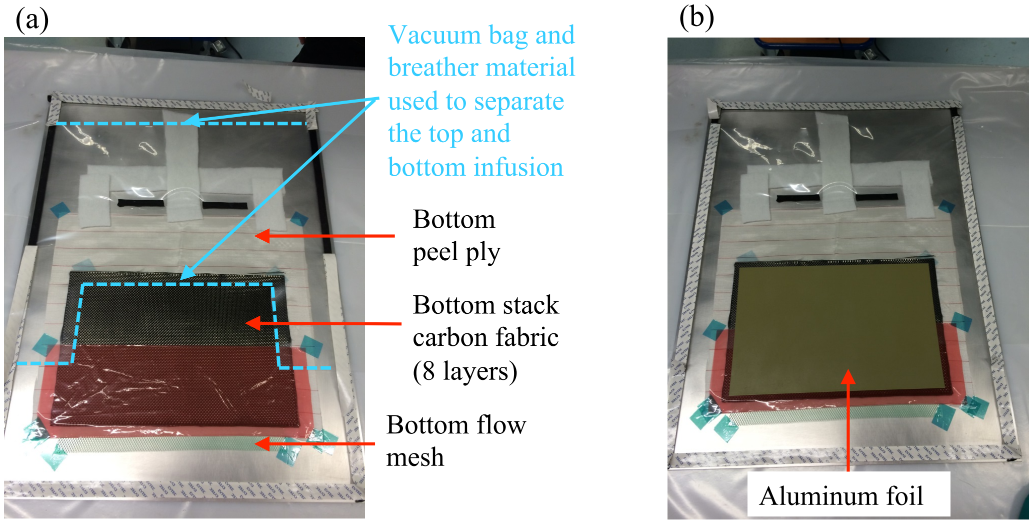

Figure 1: (a) Panel layup for bottom part (b) Panel layup after Al foil was assembled.

The Epikote 04908 resin and Epikure 04908 hardener, both of which are in liquid form at room temperature, were mixed with a resin-to-hardener ratio of 100:30 and then degassed under full vacuum for 20 minutes. Infusion of the degassed resin into the panel preform was performed under 50 mbar vacuum. When the resin fronts of both top and bottom flows were observed outside of the panel preform, a vacuum reduction was performed. The vacuum pump read 300 mbar during this reduction. The resin mixing, degassing and infusion steps were all done at room temperature. Once infusion was completed, the panel was cured at 80°C for 6 hours in an oven. A vacuum pressure of 300 mbar was maintained during the entire curing cycle. Two thermocouples were placed on the top of the panel and on the plate in order to monitor the temperature during infusion and curing. Figure 2 shows the infused panel ready for curing. The resulting hybrid panel had final dimensions of 220 mm x 330 mm x 4.4 mm.

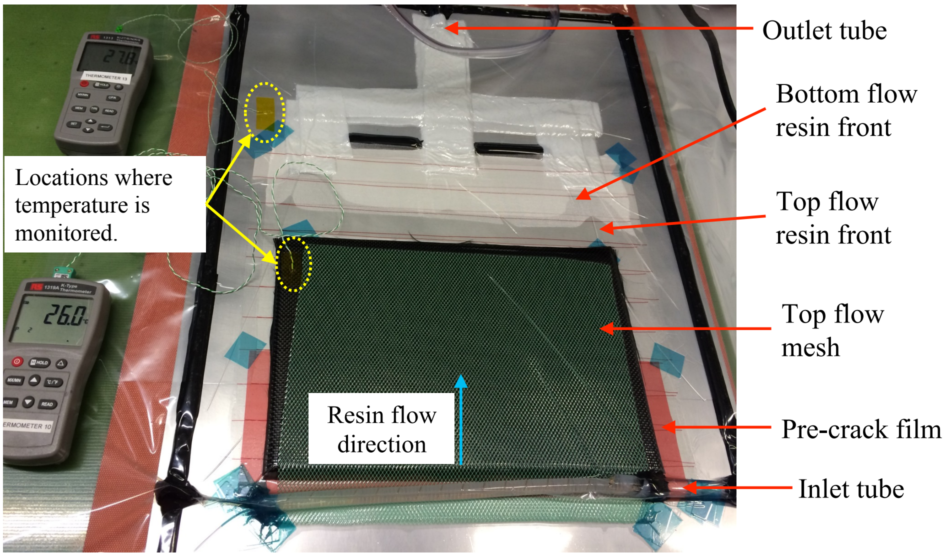

Figure 2: Infused hybrid panel.

2.3 DCB specimen preparation

Strips of 25 mm nominal width were cut from all 4 edges of the fabricated panel before cutting the DCB specimens to ensure uniform thickness in all specimens. Piano hinges were bonded onto the specimens using adhesive 3M Scotch-Weld 9323. The specimens were painted white on one edge to facilitate observation of the crack tip during testing. A scale created by millimeter paper was adhesively bonded on the painted edge of the DCB specimen to aid the measurement of the crack length.

3 DOUBLE CANTILEVER BEAM TESTS

3.1 DCB test procedure

Based on differential scanning calorimetry (DSC) measurements of the fabricated hybrid composite, the glass transition temperature (T_g) is 83.2 ± 0.9^{o}C with the lower onset of 76.5^{o}C. As a result, 60^{o}C was selected for elevated temperature investigation for the studied material system to avoid the softening of the matrix when heated near its T_g. DCB tests were carried out at 25^{o}C and 60^{o}C following ASTM D5528 guidance [10]. The loading rate for all tests was 2 mm/min with a data acquisition rate of 10 Hz. Elevated temperature tests were carried out in an environmental chamber. Thermocouples were taped to both the top and bottom sides of the specimens prior to being loaded to the test frame. Temperature of the specimen was monitored during heating and upon loading. When each elevated specimen's temperature reached 60 ± 1^{o}C, the temperature was allowed to stabilize for 15 minutes to make sure that the temperature profile in the specimen was uniform before being tested.

3.2 On-line monitoring with Rayleigh backscattering fiber optic system

Besides visual observation of the crack propagation along the side of the DCB specimen as described above, an on-line monitoring technique using fiber optics was performed during the DCB tests to provide additional information for the location of crack tip across the specimen's width. This technique is based on Rayleigh backscattering phenomenon and allows the users to measure axial strain along the specimen length. Strain measurements were obtained with a spacial resolution of 1.3 mm at a data acquisition rate of 1 Hz. The data acquisition system used for the distributed strain measurements in this study is the commercial Optical Frequency Domain Reflectometry (ODISI-B) manufactured by Luna Technologies, Inc. Comparisons between this new technique and traditional strain gauges were studied by Martinez *et al* [11]. It was shown that the two methods of strain measurements are in good agreement with each other.

In this work, Rayleigh backscattering fiber optic sensors were glued along the longitudinal edges, and both the top and bottom sides of the DCB specimen for in-situ distributed strain measurements. An example of a DCB specimen with fiber optics bonded on the surface is shown on Figure 3(a). Figure 3(b) presents a schematic of the fiber optics path on the top surface of the DCB specimen. An illustration of the test set-up with in-situ strain measurement system is shown in Figure 4.

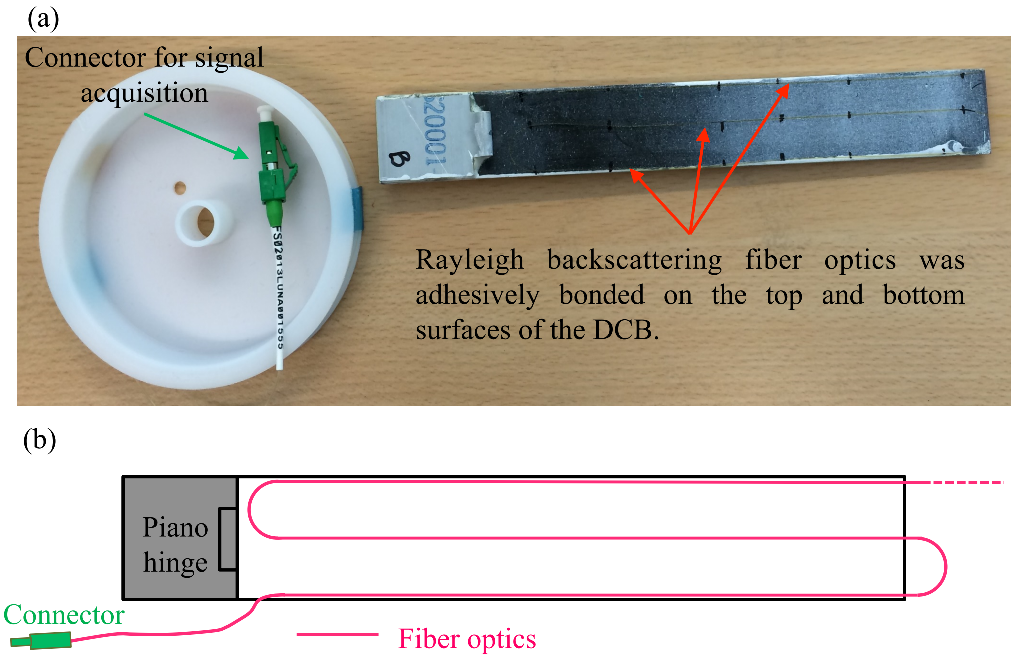

Figure 3: (a) A DCB specimen with fiber optics bonded on the surfaces (b) Top view schematic of a DCB specimen with fiber optics bonded on the surfaces.

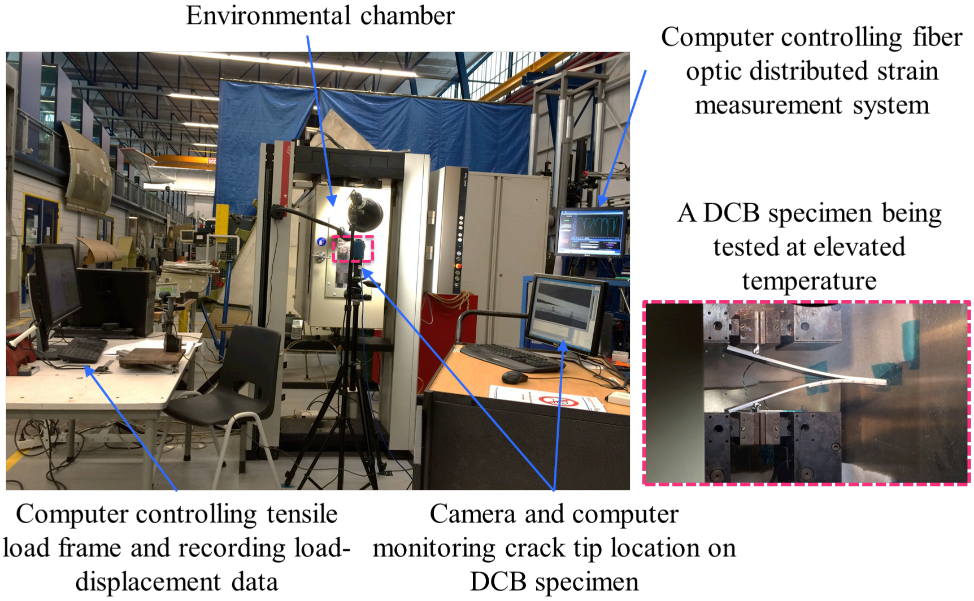

Figure 4: The DCB test setup.

4 FINITE ELEMENT ANALYSIS

Two-dimensional finite element analysis (FEA) of the hybrid DCB specimen was performed using the ABAQUS commercial FEA package. Linear elastic constitutive responses were assumed for both constituent materials in the FEA. Homogenized properties of the PMC as well aluminum 2024-T3 are summarized in Table 2. The properties of the PMC were obtained previously obtained from FE homogenization analyses of the composite at the tow and weave scales. The 1, 2, 3 local coordinate system here are along the length, thickness and width directions of the specimen respectively. Figure 5 shows a schematic of the DCB specimen's cross-section with boundary conditions used in the analysis. Quadratic plane strain (CPE8) elements were used in the entire model. The nonlinear geometric option in ABAQUS was selected to take into account the effect of large deformation. The ABAQUS built-in virtual crack closure technique (VCCT) with the B-K fracture criterion was used to analyze the crack propagation behavior of the hybrid DCB specimen [12]. The critical mode I strain energy release rate input was obtained from the experiment. Mode II and mode III fracture toughness was assumed to be the same as the mode I value.

	Engineering constant	Unit	Value
Homogenized plain weave T300 carbon fabric epoxy composite	$E_1 = E_3$	[GPa]	56.5
	E_2	[GPa]	10.6
	$\nu_{12} = \nu_{23}$	–	0.392
	ν_{13}	–	0.148
	$G_{12} = G_{23}$	[GPa]	3.13
	G_{13}	[GPa]	4.13
	$\alpha_{11} = \alpha_{33}$	$(^{o}C)^{-1}$	2.17×10^{-5}
	α_{22}	$(^{o}C)^{-1}$	-3.62×10^{-7}
Aluminium 2024-T3	E	GPa	72.4
	ν	–	0.33
	G	GPa	27.6
	α	$(^{o}C)^{-1}$	22×10^{-6}

Table 2: Material properties used in finite element analysis.

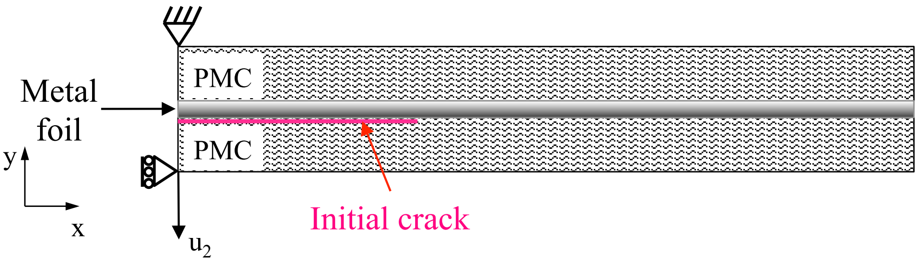

Figure 5: Cross-section view schematic of a DCB specimen with boundary conditions (not to scale).

5 RESULTS AND DISCUSSION

5.1 Mode-I dominant fracture behavior

Typical load-displacement curves measured from the DCB tests both at 25°C and 60°C are presented in Figure 6. Unstable crack propagation, i.e. the repeated crack advancing and arresting behavior due to the weave architecture in the PMC, is observed at both room and elevated temperature as indicated by the saw-tooth behavior in the load-displacement curves. In addition, at 60°C, delamination at the hybrid interface is more unstable than at 25°C. This is revealed by the larger saw-tooth patterns in the load-displacement curves from tests at 60°C compared to the patterns observed from test load-displacement curves at room temperature. At elevated temperature, the crack propagates longer distances and there are fewer number of crack propagations in comparison with crack progression behavior at room temperature.

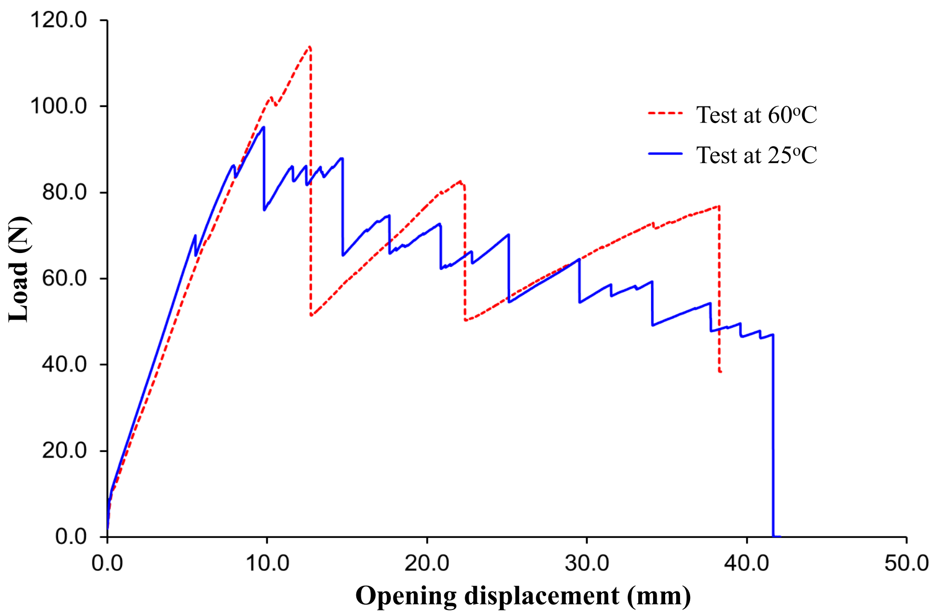

Figure 6: Typical load-displacement curve for DCB tests at 25°C and 60°C.

From the FEA results, the ratio of mode-II to mode-I strain energy release rates was calculated to be 3.1%. Thus, G_I values for the hybrid interface in this study were calculated assuming a symmetric configuration and in accordance with ASTM D5528 standard [10]. The modified beam theory expression to calculate the mode-I dominant strain energy release rates is as follows:

$$G_I = \frac{3P\delta}{2ba}, \quad (1)$$

where P is the applied load, δ is the opening displacement, b is the specimen width and a is delamination or crack length.

The calculated mode-I dominant strain energy release rate values for DCB tests performed at both 25°C and 60°C are shown on Figure 7. It is observed that fracture toughness of the hybrid interface at 60°C is higher than that at 25°C.

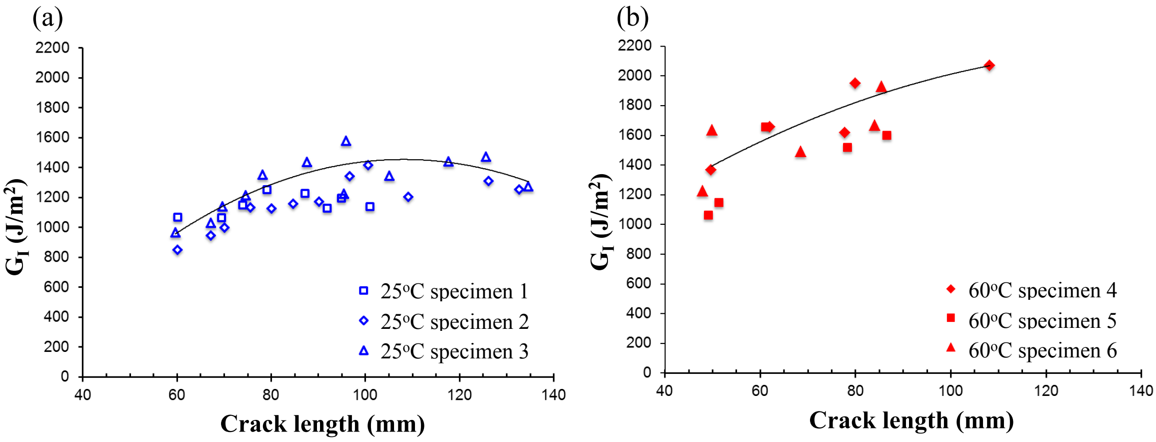

Figure 7: Mode-I dominant strain energy release rate values for DCB tests at (a) 25°C and (b) 60°C.

5.2 Distributed strain measurement results

Figures 8 and 9 show the distributed strain on the topside along the length of the DCB specimen using the Rayleigh backscattering fiber optics measurement system at 25°C and 60°C respectively. In bending, the top and bottom sides of the loaded DCB specimen are under compression. Thus, negative strain values are obtained. It is observed that along the specimen's length, the compression strain magnitude increases from the delaminated end of the beam, or the loading pin, to the vicinity of the crack tip, where the maximum compression strain value was measured, and then immediately decays to zero strain. It should be noted that these distributed strain measurement data were acquired at a rate of 1 Hz; hence, there are multiple sets of data obtained for each crack tip location. For the sake of visualization clarity, only the data sets at critical times, i.e. right before and right after the crack propagates are plotted in Figures 8 and 9 for the first few crack lengths.

Illustrations of the crack growth-arresting are shown in Figures 8(b) and 9(b). The evolution of crack progression follows the arrows drawn in these figures. As the crack tip experiences a critical strain value, the strain energy is released and the crack tip moves to a new location as demonstrated by the solid arrows. At this new location, the magnitude of the compression strain that the crack tip undergoes a reduction of an amount in the range of 100 x 10^{-6} to 600 x 10^{-6}. This strain value then gradually increases to a critical value following the trend shown by the dashed arrows, then the strain energy is released again and the crack propagates accordingly. The data points representing the locations of crack tip and critical strain values are highlighted in Figures 8(b) and 9(b). This crack growth-arresting behavior repeats until the specimen is fully delaminated. The behavior observed from the distributed strain measurements supports the saw-tooth patterns seen earlier on the load-displacement curves. In addition, crack tip locations measured by fiber optics are in good agreement with those visually observed.

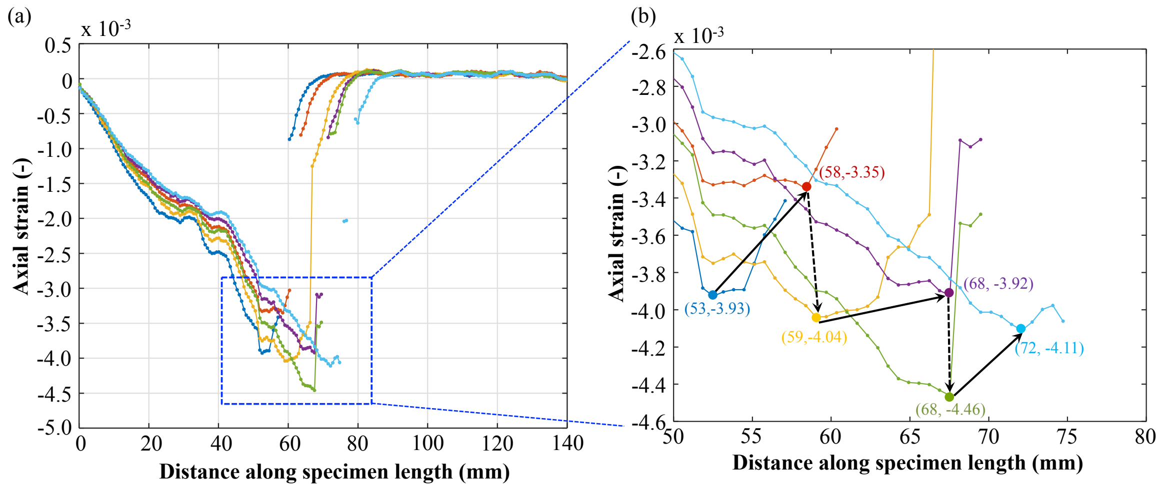

Figure 8: Distributed strain measured by fiber optics during a DCB test at 25°C.

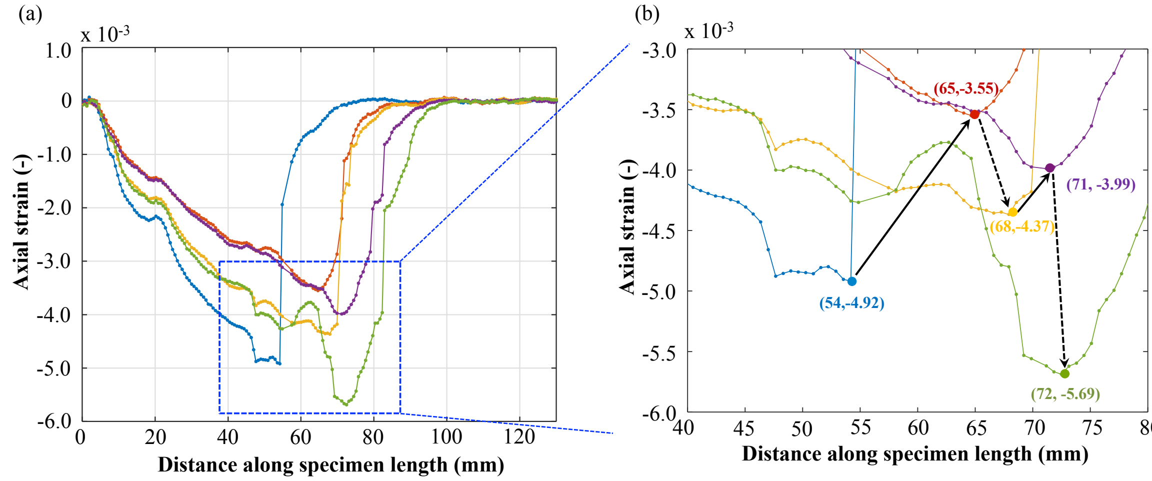

Figure 9: Distributed strain measured by fiber optics during a DCB test at 60°C.

5.4 Finite element analysis results

Axial strain profiles obtained from finite element analysis on the topside of the DCB specimen at different time frames in the analysis are shown on Figure 10. The dashed arrow on Figure 10 shows the evolution of strain profiles when the crack tip is at initial location. Similar to what was observed in the experiment, the compressive strain values gradually decrease as the specimen is loaded. Once the critical value is reached, the delamination starts to progress. However, the crack propagation observed in the analysis does not exhibit the growing-resetting behavior as seen previously in the experiment. The critical strain values remains almost constant as the crack propagates following the trend indicated by the solid arrow on Figure 10. The crack progression demonstrated in the analysis is smooth, thus, representing a stable crack growth. This is because in the analysis, the delamination occurs on a straight interface between the metal and PMC, while in reality, the weave architecture plays an important role on crack propagation behaviour.

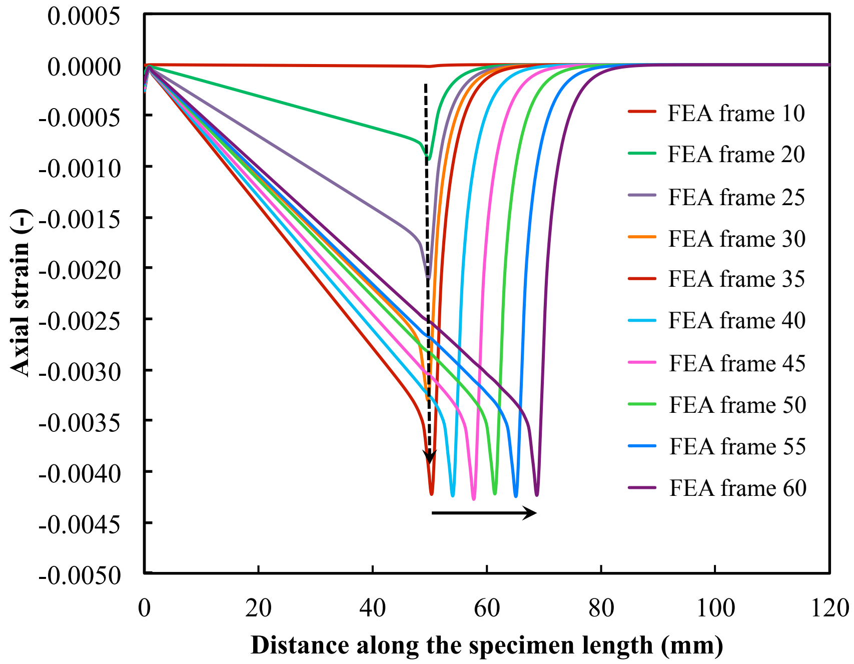

Figure 10: Strain profiles obtained from FEA on the topside of the DCB specimen at different time frames in the analysis.

Results from FEA show good agreement with experimental data for load-displacement curve and fiber optic measurements. As shown in Figure 11(a), the analysis captures the maximum load and displacement at failure as seen in the experiment. Again, it is confirmed that smooth (stable) crack propagation is observed in FEA in contrast to the saw-tooth pattern on the curve obtained experimentally. Figure 11(b) shows strain profiles obtained along the top edge of the DCB specimen. As part of our future work in this field, on-going computational effort is being carried out to study mesh sensitivity as well as effect of elevated temperature and weave architecture presented at the hybrid metal-PMC interface. In addition, the effect of residual stress introduced during the curing cycle will be taken into account by adding an analysis step before the loading step in the DCB model. Furthermore, three-dimensional analyses will be carried out to explore the propagation behavior across the width of the double cantilever beam.

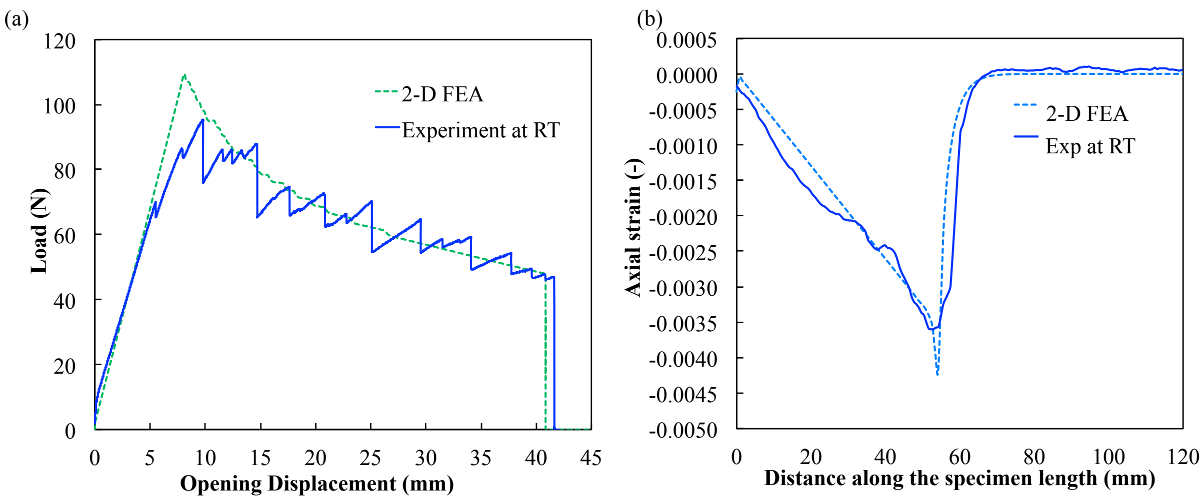

Figure 11: Comparison between experiment done at RT and FEA for (a) load-displacement curve (b) distributed strain profile right before the crack propagates when the crack tip is at the initial location.

6 CONCLUSIONS

In this work, an effective out-of-autoclave manufacturing method, VATRM, was used to create a hybrid composite laminate that is composed of a layer of aluminum foil placed at the center of sixteen layer plain-weave carbon fabric with epoxy matrix. The hybrid interface between aluminum foil and the PMC was created by co-curing and without the use of any additional adhesive. The fracture behavior of the fabricated hybrid interface was investigated at both room and elevated temperature. It was observed that the crack propagation behavior at the hybrid interface is more unstable at elevated temperature compared to that at room temperature. The strain energy release rates required for the crack to propagate at elevated temperature is higher than that needed at room temperature. In addition, for the first time, in-situ Rayleigh backscattering fiber optics measurements were obtained during DCB experiments. This new technique to measure distributed strains allows us to interpret the DCB experiment in a new way and enables the visualization of strain energy release upon crack propagation. Two-dimensional finite element analysis was carried out and validated with experiment via both load-displacement curves and axial strain profiles. The two-dimensional simulation was able to capture the behavior observed experimentally. Current three-dimensional analyses are underway to study the effect of residual stresses, elevated temperature and the reinforcement woven architecture of the PMC on the delamination behavior of the hybrid metal-PMC interface.

ACKNOWLEDGEMENTS

The authors would like to acknowledge the financial support by the NASA Space Technology Research Fellowship Grant No. NNX14AM41H, the AFOSR MURI Award No. FA9550-09-1-0686, and the International Institute for Multifunctional Materials for Energy Conversion (IIMEC) established by NSF Grant No. DMR-0844082.

REFERENCES

[1] A. Vlot, J.W. Gunnink, *Fibre metal laminates: an introduction*, Springer Science & Business Media, 2001.

[2] C. Lin, P. Kao, Effect of fiber bridging on the fatigue crack propagation in carbon fiber-reinforced aluminum laminates, *Materials Science and Engineering: A*, **190**, 1995, pp. 65-73.

[3] C. Lin, P. Kao, Delamination growth and its effect on crack propagation in carbon fiber reinforced aluminum laminates under fatigue loading, *Acta materialia*, **44**, 1996, pp.1181-8.

[4] H. Ning, Y. Li, N. Hu, M. Arai, N. Takizawa, Y. Liu *et al*, Experimental and numerical study on the improvement of interlaminar mechanical properties of Al/CFRP laminates, *Journal of Materials Processing Technology*, **216**, 2015, pp. 79-88.

[5] H. Ning, T. Iijima, N. Hu, Y. Liu, L. Wu, F. Liu, *et al*, Investigation on mode-II interface fracture toughness of CFRP/Al laminates toughened by VGCF interleaves, *Journal of Materials Science*, **50**, 2015, pp. 1915-23.

[6] M. Banea, R. Campilho, Mode II fracture toughness of adhesively bonded joints as a function of temperature: experimental and numerical study, *The Journal of Adhesion*, **88**, 2012, pp. 534-51.

[7] M. Banea, R. Campilho, Effect of temperature on tensile strength and mode I fracture toughness of a high temperature epoxy adhesive, *Journal of Adhesion Science and Technology*, **26**, 2012, pp. 939-53.

[8] H.T.X. Truong, D.C. Lagoudas, O.O. Ochoa, K. Lafdi, Fracture toughness of fiber metal laminates: Carbon nanotube modified Ti–polymer–matrix composite interface, *Journal of Composite Materials*, **48**, 2014, pp. 2697-710.

[9] R. Krueger, A summary of benchmark examples to assess the performance of quasi-static delamination propagation prediction capabilities in finite element codes. *Journal of Composite Materials*, 2014, doi:0021998314561812.

[10] ASTM Standard, *Standard test method for mode I interlaminar fracture toughness of unidirectional fiber-reinforced polymer matrix composites*, ASTM Standard D, 5528, 2013.
[11] M. Martinez, A. Beltempo, M. Yanishevsky, R. Rutledge, B. Rocha, Load monitoring on SHM platform 1A using LUNA Technologies, distributed sensing fibre optic system, *Unclassified Lab Technical Report LTR-SMPL-2012-0047*, National Research Council of Canada, 2012.
[12] ABAQUS Documentation, Version 6.14, *Dassault Systemes*, 2014.